Near Surface Boreal Summer Climate as Simulated by Three General Circulation Models

Paul A. Dirmeyer

Michael J. Fennessy

L. Marx

Center for Ocean-Land-Atmosphere Studies

4041 Powder Mill Road, Suite 302

Calverton, MD 20705

e-mail: dirmeyer@cola..iges.org

June 2001

Abstract

Ensemble integrations of three general circulation models (COLA, NCAR and NCEP) have been performed over five different boreal summer seasons (June through September of 1986, 1987, 1988, 1993 and 1994) with prescribed observed sea surface temperature to assess the predictability of seasonal climate during the boreal summer. Beyond some inconsistent initialization of soil wetness among the models, there is no land surface contribution to predictability that can be assesed. An evaluation of the systematic errors of the models shows strikingly similar patterns among them. Despite large systematic errors, aspects of the time evolution of climate during the boreal summer are well simulated, with particular attention paid in this analysis to the major monsoon regions of Asia and North America. Potential predictability is assessed by examining in tandem the models' skill as measured by their anomaly correlation coefficients, and the models' signal to noise ratio (essentially interannual versus intra-ensemble variance) as a measure of confidence in the results. Co-location of skill in anomaly simulation and a robust signal is a strong indicator of potential predictability. Predictability of interannual climate variations is found to be low outside the deep tropics. Useful predictability of precipitation over land is found consistently only over Indonesia. There is some extratropical skill in simulating surface temperatures, particularly over North America, but not all models show potential predictability. Predictability appears strongest in June, probably due to the influence of the initial conditions. With only SST as a driving boundary condition, the poor performance of these models during summer may indicate that we must turn to the land surface in order to harvest potential predictability.

1. Introduction

Dynamical Seasonal Prediction (DSP) is a multi-institutional research project to examine the predictability of the earth's climate on the seasonal timescale. Dynamical prediction implies the use of physically-based numerical models like those used for numerical weather prediction, as opposed to statistical techniques that have historically been used for climate prediction. A special issue of the *Quarterly Journal of the Royal Meteorological Society* (2000: 126, 1989-2350) was recently dedicated to DSP and its sister project in Europe called PROVOST (PRediction Of climate Variations On Seasonal-interannual Timescales).

The hypothesis behind DSP is that it is now feasible to extend the capabilities developed for numerical weather prediction to the seasonal scale using state-of-the-art global models of the atmosphere and land surface. Initial atmospheric conditions at the beginning of the season may provide some skill, as there is some "memory" in the atmosphere that persists for several weeks. However, the bulk of the memory of the climate system on seasonal scales comes from the surface boundary — the ocean and land. Sea surface temperature (SST) varies slowly, and may be predictable at a useful level of skill up to a year in advance (Kirtman et al. 1997). Soil moisture, snow cover, and the state of vegetation act as agents of climate memory at the land surface. It is believed that predictability at seasonal timescales will come from the memory inherent in the ocean and land.

To date, the DSP project has focused on climate predictability during the boreal winter season (Shukla et al. 2000). Given the well documented impact of the El Niño / Southern Oscillation (ENSO) on the Pacific-North America (PNA) region during boreal winter, this season was a logical place to begin looking for skill. Whereas the response in the tropics to anomalous surface boundary conditions is usually quite vigorous and potentially predictable (Charney and Shukla 1981), in the mid-latitudes the signal can be engulfed by the

noise of synoptic-scale baroclinic systems. The PNA region during winter is an exception, particularly when tropical SST anomalies are large (Shukla 1998).

Why should winter climate be predictable in the PNA region more than elsewhere? There is no definitive answer, but its proximity and orientation relative to the tropical Pacific ocean, where the El Niño SST fluctuations take place, appear to put it downstream of the large-scale wavetrain emanating from that equatorial region of anomalous heating (Shukla and Wallace 1983, Rasmusson and Wallace 1983). The mean state of the general circulation affects the refraction of such wavetrains, determining their paths and strength (Hoskins and Karoly 1981).

Climate during boreal summer appears to be somewhat less determined by tropical ocean forcing, but SST may still play an important role (Trenberth et al. 1988, Palmer and Brankovi*ƒ* 1989, Mo and Paegle 2000). During summer in the subtropics and mid-latitudes, land surface conditions may act to modulate the response of the atmospheric circulation to SST anomalies (Fennessy et al. 1994), and errors in land surface state variables such as soil wetness can degrade climate simulations (Dirmeyer 2000). The atmosphere is not decoupled from the land as in winter, so land surface fluxes can provide a local feedback to climate anomalies (Reale et al. 2001).

In this paper, we examine the results of a boreal summer rendition of DSP. This experiment is more limited in scope than the winter DSP, using three of the same climate models and covering only five years. Nonetheless, it provides a glimpse into SST-forced predictability during summer. Section 2 describes the models and the summer experiment. A discussion of the simulation of mean boreal summer climate is given in section 3. In section 4, the ability of the models to reproduced observed interannual variations is assessed. Conclusions are given in section 5.

2. Models and Experiment

Three global general circulation models (GCMs) were integrated at COLA as part of the DSP project. The National Centers for Environmental Prediction (NCEP) GCM is similar to the model used for the NCEP/National Center for Atmospheric Research (NCAR) reanalysis (Kalnay et al. 1996). It was run at a spectral resolution of T62 (1.9E) with 28 vertical levels. The NCAR Community Climate Model Version 3 (CCM3; Kiehl et al. 1998) was run at T42 resolution (2.8E) with 19 levels. The COLA GCM (Kinter et al. 1997) was integrated at a resolution of R40 (1.8E×2.8E) with 18 vertical levels.

While the DSP project focused on the boreal winter season, some summer simulations were also made. Initial atmospheric conditions for all summer integrations were taken from the NCEP/NCAR reanalyses on the last days of May, in the years 1986, 1987, 1988, 1993 and 1994. The COLA GCM ensembles contain nine members, the NCEP and NCAR GCM ensembles have five members each. The models are integrated through the end of September. Monthly mean statistics were retained, and are compared in the following sections.

In these integrations, the NCEP GCM land surface is initialized from the NCEP/NCAR reanalysis land surface state (Kalnay et al. 1996). The COLA GCM soil wetness comes from a calculation based on the operational analysis of the European Centre for Medium-range Weather Forecasts (ECMWF) as described by Fennessy and Shukla (1999). The NCAR CCM3 model uses climatological initial conditions at the land surface. All models initialize soil temperatures and snow cover from climatological values.

All runs use a common data set for sea surface temperature (SST), namely the OISST data set of Reynolds and Smith (1994). Thus, the simulations can be thought of as an exercise in seasonal climate forecasting

with perfect knowledge of the evolution of the ocean state. The DSP historical seasonal forecasts represent something of an upper estimate of the skill attainable from SST forcing by current climate models. Encouraging skill has been found during boreal winter (Shukla et al. 2000). In this paper, the skill during summer will be assessed.

3. Mean Climate

Figure 1 shows the seasonal mean (June through September) global precipitation from the CPC Merged Analysis of Precipitation (CMAP; Xie and Arkin 1997) data set for the five years of summer integrations, and the systematic errors of each of the models during this time period. All three models overestimate the global mean precipitation rate for this period. In the CMAP data set, the global mean rate is 2.78 mm d^{-1}. The COLA, NCAR, and NCEP GCMs produce 3.86, 3.35, and 3.65 mm d^{-1} respectively.

The three models also show remarkably similar patterns of systematic error, particularly over ocean. Table 1 shows the global error correlations between each combination of models, as well as the correlations calculated over land and ocean points separately. The correlations are significant at the 99% significance level for each pairing of global and ocean-only correlations, and at the 95% level for the COLA-NCAR and NCEP-COLA pairings over land. Returning to Fig 1, each model shows an excess of rainfall over high latitude oceans in the Southern Hemisphere, and land in the Northern Hemisphere. Each shows excessive rainfall over the western tropical Atlantic, Indian Ocean, and off the equator in the Pacific. All show similar excesses over China, and overly dry conditions over India. The similarities over ocean, where each model has used the same SST boundary conditions, are particularly curious. Do each of these models suffer from the same shortcomings in their parameterizations of physical processes (e.g., convection and boundary layer

simulation), or are there perhaps problems in our estimations of ocean temperatures relevant to climate (c.f. Vazquez-Cuervo and Sumagaysay 2001)? Or are there systematic errors in the CMAP estimates of rainfall over ocean? Results using the Global Precipitation Climatology Project (GPCP; Huffman et al. 1997) data set give virtually identical results as those shown in Fig 1. It is beyond the scope of this paper to try to elucidate a reason for these similarities, but it is worthy of investigation.

The similarities in errors over land are somewhat easier to explain. Uniformly poor representation of important orographic features, such as those found over the Andes, the Rockies, and the Himalayas undoubtedly account for some of the systematic errors in these regions. Many of the largest errors are in regions of mountainous terrain.

Figure 2 shows the seasonal mean surface temperature from the Climate Anomaly Monitoring Network (CAMS; Ropelewski et al. 1985) data set for the same five years, and the model systematic errors. All models again show large-scale systematic errors. The COLA GCM has a distinct warm bias over Africa, and at high northern latitudes, with cold biases over high terrain, Australia, and the Amazon basin. The NCAR CCM3 shows cold biases over most land areas, with a major exception being over the south-central United States. Temperature errors in the NCEP GCM resemble those of the COLA model, but with a slightly lower magnitudes in general. It should be noted that the versions of the COLA and NCEP GCMs used in this study share a common heritage that is quite different from the NCAR GCM. There are strong similarities in the dynamical cores of the COLA and NCEP models, that might give the expectation that their climates will resemble each other more than either would resemble that of the NCAR model. In fact, that is not entirely the case for precipitation, but over land there is a strong similarity between the systematic temperature errors of the COLA and NCEP models (see Table 1). The COLA and NCEP

models have very different land surface parameterizations, so these similarities may be a consequence of the properties of the atmospheric components of the models.

As suggested by Figs 1 and 2, all three models have similarly large root mean square errors for precipitation and temperature. These are summarized in Table 2. The COLA GCM has slightly higher errors than the other two models, and all three models show lower RMS errors for precipitation averaged over land than over ocean. Compared with size of typical seasonal anomalies, shown in the next section, the mean errors are large.

Now we examine the ability of these three models to simulate key aspects of the seasonal cycle during boreal summer. Figure 3 shows the 5-year mean July minus June rainfall over the North American region. Higgins et al. (1997) has shown that the North American monsoon onset occurs around the beginning of July, and that there is a profound shift in the precipitation regimes, not only over the southwest coast of North America, but also over the southern Great Plains. The observed rainfall difference shows a distinct east-west dipole spanning approximately 100EW, with increasing rainfall over the Pacific sector, and a decrease over the Gulf of Mexico and Atlantic sectors including Central America. The COLA and NCAR GCMs capture the terrestrial part of this pattern fairly well outside the tropics, but do a poor job over the ocean east of North America and in the deep tropics. The NCAR model has generally larger errors, but it does capture the drying over the southern Great Plains and the wetter Southeast U.S. associated with the strengthening of the Bermuda ridge better than the COLA GCM. The NCEP model produces a predominantly north-south dipole over Mexico and the United States, but is alone in simulating the drying over the eastern Gulf of Mexico. None of the models extend the rains of the North American monsoon northward into Arizona and New Mexico, and all struggle to represent the extent of increased rainfall over

the eastern tropical Pacific, possibly due to their inability to simulate properly tropical cyclones at these resolutions.

Figure 4 shows a similar analysis over the Asian monsoon region. The July minus June difference shows the establishment of monsoon rains over the Indian subcontinent and into southern China and the Philippines, drying over the Arabian Sea, coastal Burma, Indonesia and southeast China, and another band of increased rainfall from Mongolia across Manchuria to Korea. All of the models show the increased monsoon and Manchurian rainfall patterns to some degree, with strong drying over the Arabian Sea. But all of the models intensify rainfall too much in the region of Nepal, with a rain shadow over Assam, likely due to problems with representation of the steep orography. Only the NCEP GCM, with the highest zonal resolution of the three models, shows a distinct band of rainfall over the Western Ghats. All of the models struggle with the details, such as the placement of the drying over southeastern China. It is difficult to say that one model does notably better or worse than the others.

4. Interannual Variability

a. Evolution of skill

The real target for DSP is assessment of predictability of intraseasonal to seasonal climate anomalies. Figure 5 shows how the ensemble mean spatial anomaly correlation coefficient (ACC) for surface temperature evolves from month to month during the boreal summer. ACC is calculated for each month, and then averaged over the five years. The top panel is for all global land points, and the bottom panel is for the North American sector alone. Globally, there is a clear degradation in skill from the first month of the integrations to later months. This degradation is evident in regional assessments over Africa and

southern Asia as well (not shown). Over North America, there is a decrease in skill from June to July, followed by an increase in the second half of the integration period. This subsequent increase is weakest for the NCEP GCM. All models show similar skill in the anomaly correlation coefficient for the four-month seasonal mean. The degradation is probably related to the gradual loss of the information contained in the initial conditions over the course of the first month as model errors grow and saturate. The reason for the increase in skill over North America going into autumn is less obvious. It may be correlated to the beginning of the transition to the wintertime circulation regime, when tropical SST may exert more control over the mid-latitude circulation.

A multi-model ensemble constructed from the mean of the three model ensembles is also plotted for each month and for the season. The multi-model ensemble is nearly always better than any of the members. Even for individual years (not shown), the multi-model ensemble ranks first or second among the four entries. Thus it appears that just as constructing an ensemble mean improves the simulation by a given climate model, ensembling across models may improve skill further, consistent with other similar investigations (e.g., Doblas-Reyes et al. 2000, Krishnamurti et al. 2000).

Figure 6 shows the ensemble mean anomaly correlation coefficients for precipitation, in the same manner as Fig 5. For global precipitation, three categories are shown: land, ocean, and total. The decay of skill gained from the initial condition is too rapid over land to show up in precipitation at the monthly time scale. However, over ocean there is some evidence of inertia from the initial atmospheric conditions. Skill is generally at a minimum in July, and increases in August and September. Again, this may reflect a change in the annual cycle of basic predictability of the climate system, as all three models show a similar behavior. Skill over ocean exceeds skill over land. Over North America, skill is minimum during the first month in

all models, and increases to a peak in August before declining somewhat in September. The skill of the multi-model ensemble in precipitation is notable, although not as impressive as for surface temperature.

b. Regional anomalies

There are certain well-known regional climate events that occurred during the seasons simulated. How well did the models reproduce these anomalies? Fig 7 shows the anomaly in surface temperature during the drought and heat wave over North America during the summer of 1988 in the CAMS temperature data and as simulated by the three models. Anomalies are calculated for June and July only, relative to the mean of the remaining four years. The warm anomaly is very prominent in the observations over a broad area of southern Canada and the northern United States, stretching from the West Coast to the Great Lakes and Hudson Bay. Each of the models produces a warm anomaly that is weaker by at least a factor of two, and displaced to the east relative to observations. It is remarkable how similar the models are to each other. Two of the models represent the cold anomaly along the Northwest coast, with the NCAR model doing the better job.

The year 1988 saw a severe drought over North America, and 1993 was a year of flooding. The difference in rainfall between the flood and drought years during June and July is shown in Fig 8. It should be noted that in fact the two events did not occur at precisely the same time of year. The drought of 1988 was concentrated mostly during spring, and had begun to abate by July, as rainfall began to return to normal over much of the central United States. The floods of 1993 were largely concentrated during a 4-5 week span from mid-June to mid-July. The observed differences show the heart of the signal to be over the Missouri and upper Mississippi river valleys. There are also widespread differences of the opposite sign over the western Atlantic Ocean, Gulf of Mexico, Greater Antilles, Central America and northern South

America. A dipole reflecting a shift in the latitude of the ITCZ over the eastern Pacific Ocean between the two years is evident as well. The models give some representation of the mid-latitude terrestrial signal with errors in position and reduced magnitude. The NCEP model does the best job of reproducing the position and magnitude of the extremum over the central U.S., perhaps as a consequence of its soil moisture initialization. However, the NCEP model also simulates other extrema over the eastern Great Lakes, Southeast coastline and the Prairie Provinces that are not evident in the CAMS station data. The COLA GCM places the anomaly too far to the south, and the NCAR model produces a very weak and diffuse response. None of the models do well in simulating the patterns over the Atlantic off the coast of North America. However, all models do rather well in simulating the patterns south of about 25EN. Not only is the dipole of the extreme eastern Pacific ITCZ captured, but the dry 1993 versus 1988 over Southern Mexico, Mesoamerica and the Greater Antilles is well captured. Even the small positive anomalies in the Caribbean Sea are represented in each model. It seems that there is more skill at low latitudes than at mid-latitudes in these models. This will be examined further below.

1987 and 1988 were also contrasting years for surface hydrology over India and the Sahel. 1988 was unusually wet in both regions (actually over the Sahel, which had been suffering through an extended drought, 1988 rainfall was near normal). 1987 saw a failed monsoon over India and severe drought in the Sahel. These oscillations are evident in the difference maps for these regions (Figs 9 and 10). Fig 9 also shows similar year-to-year variations in rainfall over Indonesia, and opposite variations over much of Indochina, especially along the coast of Burma. None of the models do a credible job of simulating the interannual fluctuation of the monsoon rain over the Indian subcontinent. Yet all three models do appear to resolve the fluctuations over the Burmese coast and Indonesia. But other maritime areas are poorly

simulated (e.g., the Philippine Sea). There also appears to be some positive signal over central China. But overall, the performance of the models is poor.

Over sub-Saharan Africa (Fig 10), the COLA and NCEP models appear to do a fairly good job of capturing the observed fluctuation of rainfall between the two years, including the contrapuntal signal along the Guinea Coast. The NCAR model does not appear to capture the signal well, perhaps due to the effect of a rather broad erroneous precipitation event over Arabia. Again, the areas where skill over land seems to be most apparent are at low latitudes. Yet over the Atlantic the three models produces a dipole pattern much more similar to each other than to the observed pattern in the CMAP data set.

It should be pointed out that while using an ensemble mean to predict climate improves a model's ability to capture anomaly patterns, by reducing the contribution of model noise in the solution, the capacity to reproduce extreme anomalies is strongly curtailed. Extreme climate anomalies in the real world may not be purely a function of the boundary conditions, but may be the result of a favorable superposition of boundary-forced response and internal atmospheric variability. The ensemble averaging that serves to enhance the boundary forced signal also suppresses the internal noise. The year-to-year variance of a single realization of a non-linear system will be reduced systematically as larger and larger ensembles are considered, so the ensemble will not have the same temporal variance statistics as a single integration. This may explain the propensity of the models to underforecast the relative strength of anomalies. However, because each model has a stronger hydrologic cycle than is observed (i.e., generally higher rainfall rates), there is some compensation when viewing the absolute magnitudes of simulated anomalies.

c. Assessment of potential predictability

In order to assess the potential predictability of the ensemble hindcasts in capturing the prominent year-to-year climate anomalies we examine an additional characteristic of the simulations. An assessment of the signal-to-noise ratio (SNR), calculated from the variance statistics of each model for key fields, reveals when and where a model may exhibit predictability. However, predictable behavior in a climate model is not of much use if the model does not exhibit skill in simulating the interannual variability at that location. We use temporal ACC as a measure of models skill. If high ACC is co-located with a high SNR for a given variable, we may presume that the model possesses useful forecast ability at that location. Low SNR does not preclude useful forecast ability, but it may lower our confidence when the model is used in an actual forecast mode.

As described in Shukla et al. (2000), the noise for a given variable is calculated as the intra-ensemble variance for each season, averaged over the five years. The signal is the variance of the ensemble means from the grand mean, with account taken for the noise component since the ensembles are of finite size. Figure 11 shows the noise and signal separately for the June-September average precipitation for each model. On the panels showing signal, the region where signal exceeds noise is outlined with a bold cyan contour. Several features are evident among the models. First, the signal in each model is largely confined to parts of the tropical oceans, with very little signal in the mid-latitudes of either hemisphere or over land. Second, regions of high noise cover a much larger area than the regions of high signal for every model. The pattern of noise is quite similar to the overall pattern of precipitation variance, or the mean precipitation for that matter. Third, each of these models shows a distinct combination of signal and noise consistent with the findings for winter described by Shukla et al. (2000). That is, the NCAR model shows noticeably less intra-ensemble noise than the other two models, while the COLA GCM shows the strongest signal. None of the models show much SNR greater than unity outside the deep tropics of the Pacific Ocean. There is

no evidence of predictability over the Asian monsoon region, for instance, in these cases. This may have something to do with the long averaging period. When shorter periods are examined, the area of useful SNR increases for each model (not shown). Monthly statistics will be examined later in this section.

Figure 12 shows the corresponding ACC calculated relative to the CMAP precipitation for the same seasonal period. The fields are very patchy, due to the small number of cases, but it can be seen that the areas where SNR exceeds one in each model correspond well with coherent regions of significant ACC. One exception is the area over southern Mexico and the adjacent ocean where the COLA model shows high SNR, but no skill in capturing the observed interannual variability. This appears to be a region where the model varies robustly, but incorrectly, on interannual time scales.

Figure 13 shows the corresponding SNR analysis for surface air temperature. Noise is prevalent across nearly all land areas, except for the deep tropics, for all three models, as well as over the Northern Hemisphere storm tracks downstream from North America and Asia where large continental air masses are advected over ocean. Signal is very weak over land and is dwarfed by noise. Over ocean (not shown), all three models show a similar signal, because of the use of identical SST. The ACC analysis (Fig 14) is more encouraging, with both the COLA and NCAR models showing skill in representing summer season temperature over a large fraction of North America. Both models also show areas of high ACC over significant parts of Asia, South America and Australia.

Much of the variation in climate anomalies of precipitation and temperature do not persist for 3–4 months, but are more evident on a monthly time scale. Figure 15 shows the ability of each model to simulate monthly temperature anomalies and the SNR at this time scale. Grey shaded areas have neither a SNR greater than unity nor an ACC significant at the 95% confidence level (no calculations have been performed

over ocean regions). The COLA model shows the highest overall SNR, but all three models have large areas of significant ACC. Areas of central and northwestern North America consistently appear as regions of high ACC in all three models. High ACC over northern Asia shows up prominently in all models during June, and there is a clear decay with time of otherwise strong SNR in the COLA model over Greenland and Antarctica. These are all manifestations of the thermal inertia exhibited by snow and ice, which results in extra persistence of the initial conditions. Similarities in the ACC between models in June over other regions, such as the mid-latitudes of South America, are probably also due to the influence of the initial conditions. All models seem to lose what high extratropical SNR they have over the course of the season, retaining relatively large signals only in the tropics.

Areas which combine high SNR with significant ACC have the greatest potential climate predictability. For the COLA model, there appears to be some potential for temperature over central North America, particularly during June, and in the same month over the Ob and La Plata river basins. The La Plata basin is also potentially predictable for the other two models. But overall, there is disappointingly little land area that appears to be predictable by any of these models.

A similar combined analysis of monthly precipitation (Fig 16) is no more promising. Outside of Indonesia, there is little consistent potential predictability over land during these months in these three climate models. What little potential predictability of precipitation there is appears limited to the central Pacific.

Figure 17 presents the same measures of predictability in the middle troposphere for 500 hPa geopotential height. Most of the high SNR is again confined to the tropical belt. The COLA and NCEP models display stronger SNR in the first month of integration, but there is a precipitous drop in SNR for the NCEP model by July. In fact, all models show a global minimum in SNR and ACC during July. ACC is high across the

tropics in June and September. In the extratropics, there is a discernable connection between high SNR and proximity to the initial state. By September, there is virtually no useful signal outside of the tropical belt in any model. With the exception of the region of the South Pacific Convergence Zone, there are no extratropical regions that show consistently high ACC from month to month in any of the models.

5. Conclusions

An analysis of a set of summer DSP ensemble simulations by three different climate models has been presented. Large systematic errors in precipitation and terrestrial near surface air temperature are evident in all three models, and they bear a striking resemblance to one another. Nonetheless, the models do capture some of the important transitional features associated with the major boreal summer monsoon regions. Examination of the interannual and intra-ensemble statistics verifies the differences between models described for the winter DSP simulations. However, unlike winter, we find that there is very little evidence of useful predictable skill outside the deep tropics during the five years simulated.

Why are simulations for boreal summer so much poorer than those shown for winter by Shukla et al. (2000)? There are two possibilities. One is that there simply is no exploitable predictability during the summer season. The other is that there is indeed predictability, but that these models are not up to the task. This remains an open question, but evidence exists for the later conclusion. Fennessy and Shukla (2000) found that by nesting the Eta regional model over North America within the COLA GCM, skillful summer season forecasts could be attained. However, the Eta is a substantially different model than the COLA GCM, so the question remains as to why this approach provided an improved simulation. Was the advantaged gained because of increased spatial resolution, potentially superior physical parameterizations,

or the impact of the Eta model's coordinate system? Some combination of factors may be responsible. These possibilities need to be investigated further.

Certainly there are also deficiencies in how these summer DSP integrations were initialized over land. If the general circulation alone determines local anomalies, and SST determines the general circulation. then there is little hope for enhancing prediction during boreal summer by improved land surface representation. If there is warm-season predictability to be harvested from the land surface state, then it may not have been captured by this experiment. These DSP simulations do not take full advantage of the potential predictability that land surface boundary conditions may contribute. As described in Section 2, The COLA GCM initializes soil wetness from values derived from ECMWF analyses, and the NCEP model uses reanalysis values that are heavily damped to climatology. There is no interannual signal in initial soil temperature or snow cover, and none of these models have the capability to represent the interannual variability of vegetation cover or color, aerosols, etc. Observed SST was prescribed throughout these integrations, not merely as an initial condition. If the land surface state were realistically prescribed throughout the season, there might have been an alteration of surface fluxes that could further improve the simulation of climate variations. The potential impact of complete, realistic land surface initial conditions and boundary conditions also needs to be examined before a definitive statement about the potential predictability of warm season climate can be made.

Acknowledgments: The authors wish to recognize J. Shukla, E. Kalnay, and D. Baumhefner, who provided these models for summer dynamical seasonal prediction experiments. This work was supported by NSF grant ATM 9814265, NOAA grant NA96GP0056 and NASA grant NAG5-8202.

References

Charney, J. G., and J. Shukla , 1981: Predictability of monsoons. *Monsoon dynamics: Proceedings of the symposium on monsoon dynamics*, New Delhi, Dec 1977, J. Lighthill and R. P. Pearce Eds., Cambridge U. Press, 99-109.

Dirmeyer, P. A., 2000: Using a global soil wetness data set to improve seasonal climate simulation. *J. Climate*, **13**, 2900-2922.

Doblas-Reyes, F. J., M. Déqué, and J.-P. Piedelievre, 2000: Multi-model spread and probabilistic seasonal forecasts in PROVOST. *Quart. J. Roy. Meteor. Soc.*, **126**, 2035-2067.

Fennessy, M. J., and J. Shukla, 1999: Impact of initial soil wetness on seasonal atmospheric prediction. *J. Climate*, **12**, 3167-3180.

Fennessy, M. J., and J. Shukla, 2000: Seasonal prediction over North America with a regional model nested in a global model. *J. Climate*, **13**, 2605-2627.

Fennessy, M. J., J. L. Kinter III, L. Marx, E. K. Schneider, P. J. Sellers, and J. Shukla, 1994: GCM simulations of the life cycles of the 1988 US drought and heat wave. COLA Report 6, Center for Ocean-Land-Atmosphere Studies, Calverton, MD , 68 pp.

Higgins, R. W., Y. Tao, and X. L. Wang, 1997: Influence of the North American monsoon system on the U.S. summer precipitation regime. *J. Climate*, **10**, 2600-2622.

Hoskins, B. J., and D. J. Karoly, 1981: The Steady Linear Response of a Spherical Atmosphere to Thermal and Orographic Forcing. *J. Atmos. Sci.*, **38**, 1179-1196.

Huffman, G. J., R. F. Adler, P. Arkin, A. Chang, R. Ferraro, A. Gruber, J. Janowiak, A. McNab, B. Rudolf, and U. Schneider, 1997: The Global Precipitation Climatology Project (GPCP) combined precipitation dataset. *Bull. Amer. Meteor. Soc.*, **78**, 5-20.

Kalnay, E., M. Kanamitsu, R. Kistler, W. Collins, D. Deaven, L. Gandin, M. Iredell, S. Saha, G. White, J. Woollen, Y. Zhu, M. Chelliah, W. Ebisuzaki, W. Higgins, J. Janowiak, K. C. Mo, C. Ropelewski, J. Wang, A. Leetmaa, R. Reynolds, R. Jenne, & D. Joseph, 1996: The NCEP/NCAR 40-year reanalysis project. *Bull. Amer. Meteor. Soc.*, **77**, 437-471.

Kiehl, J. T., J. J. Hack, G. B. Bonan, B. A. Boville, D. L. Williamson, and P. J. Rasch, 1998: The National Center for Atmospheric Research Community Climate Model: CCM3. *J. Climate*, **11**, 1131-1149.

Kinter, J. L., D. DeWitt, P. A. Dirmeyer, M. J. Fennessy, B. P. Kirtman, L. Marx, E. K. Schneider, J. Shukla, and D. M. Straus, 1997: The COLA atmosphere-biosphere general circulation model. Volume 1: Formulation. COLA Report 51, Center for Ocean-Land-Atmosphere Studies, Calverton, MD , 46 pp.

Kirtman, B. P., J. Shukla, B. Huang, Z. Zhu, and E. K. Schneider, 1997: Multiseasonal predictions with a coupled tropical ocean-global atmosphere system. *Mon. Wea. Rev.*, **125**, 789-808.

Krishnamurti, T. N., C. M. Kishtawal, Z. Zhang, T. LaRow, D. Bachiochi, E. Williford, S. Gadgil, and S. Surendran, 2000: Multimodel ensemble forecasts for weather and seasonal climate. *J. Climate*, **13**, 4196-4216.

Mo, K. C., and J. N. Paegle, 2000: Influence of sea surface temperature anomalies on the precipitation regimes over the southwest United States. *J. Climate*, **13**, 3588-3598.

Palmer, T. N. and „. Brankovi*f*, 1989: The 1988 US drought linked to anomalous sea surface temperature. *Nature*, **338,** 54-57.

Rasmusson, E. M., and J. M. Wallace, 1983: Meteorological Aspects of the El Niño/Southern Oscillation. *Science*, **222**, 1195-1202.

Reale, O., P. A. Dirmeyer and A. Schlosser, 2001: Modeling the effect of land-surface variability on precipitation. Part II: Spatial and timescale structure. COLA Technical Report 97 [Available from the Center for Ocean-Land-Atmosphere Studies, 4041 Powder Mill Road, Suite 302, Calverton, MD 20705 USA], (accepted).

Reynolds, R. W., and T. M. Smith, 1994: Improved global sea surface temperature analyses using optimal interpolation. *J. Climate*, **7**, 929-948.

Ropelewski, C. F., J. E. Janowiak, and M. F. Halpert, 1985: The analysis and display of real time surface climate data. *Mon. Wea. Rev.*, **113**, 1101-1107.

Shukla, J. and J. M. Wallace, 1983: Numerical simulation of the atmospheric response to equatorial Pacific sea surface temperature anomalies. *J. Atmos. Sci.*, **40,** 1613-1630.

Shukla, J., 1998: Predictability in the midst of chaos: A scientific basis for climate forecasting. *Science*, **282**, 728-731.

Shukla, J., J. Anderson, D. Baumhefner, C. Brankovic, Y. Chang, E. Kalnay, L. Marx, T. Palmer, D. Paolino, J. Ploshay, S. Schubert, D. Straus, M. Suarez, and J. Tribbia, 2000: Dynamical seasonal prediction. *Bull. Amer. Meteor. Soc.*, **81**, 2593-2606.

Trenberth, K. E., G. W. Branstator and P. A. Arkin, 1988: Origins of the 1988 North American Drought. *Science*, **242**, 1640-1645.

Vazquez-Cuervo, J., and R. Sumagaysay, 2001: A comparison between sea surface temperatures as derived from the European remote sensing along-track scanning radiometer and the NOAA/NASA AVHRR oceans pathfinder dataset. *Bull. Amer. Meteor. Soc.*, **82**, 925-944.

Xie, P., and P. A. Arkin, 1997: Global precipitation: A 17-year monthly analysis based on gauge observations, satellite estimates, and numerical model outputs. *Bull. Amer. Meteor. Soc.*, **78**, 2539-2558.

	Precipitation			Temperature
	Global	Land Only	Ocean Only	Land Only
COLA vs. NCAR	0.55	0.47	0.57	0.30
NCAR vs. NCEP	0.40	0.24	0.46	0.28
COLA vs. NCEP	0.54	0.50	0.55	0.80

Table 1. Correlation of the spatial patterns of JJAS systematic error between the GCMs. Regions poleward of 80EN and 60ES have been excluded.

	Precipitation			Temperature
	Global	Land Only	Ocean Only	Land Only
COLA	2.36	2.07	2.47	3.89
NCAR	2.09	2.05	2.11	3.59
NCEP	2.31	2.00	2.42	3.56

Table 2. JJAS root mean square error. Units are mm d^{-1} for precipitation, K for temperature. Regions poleward of 80EN and 60ES have been excluded.

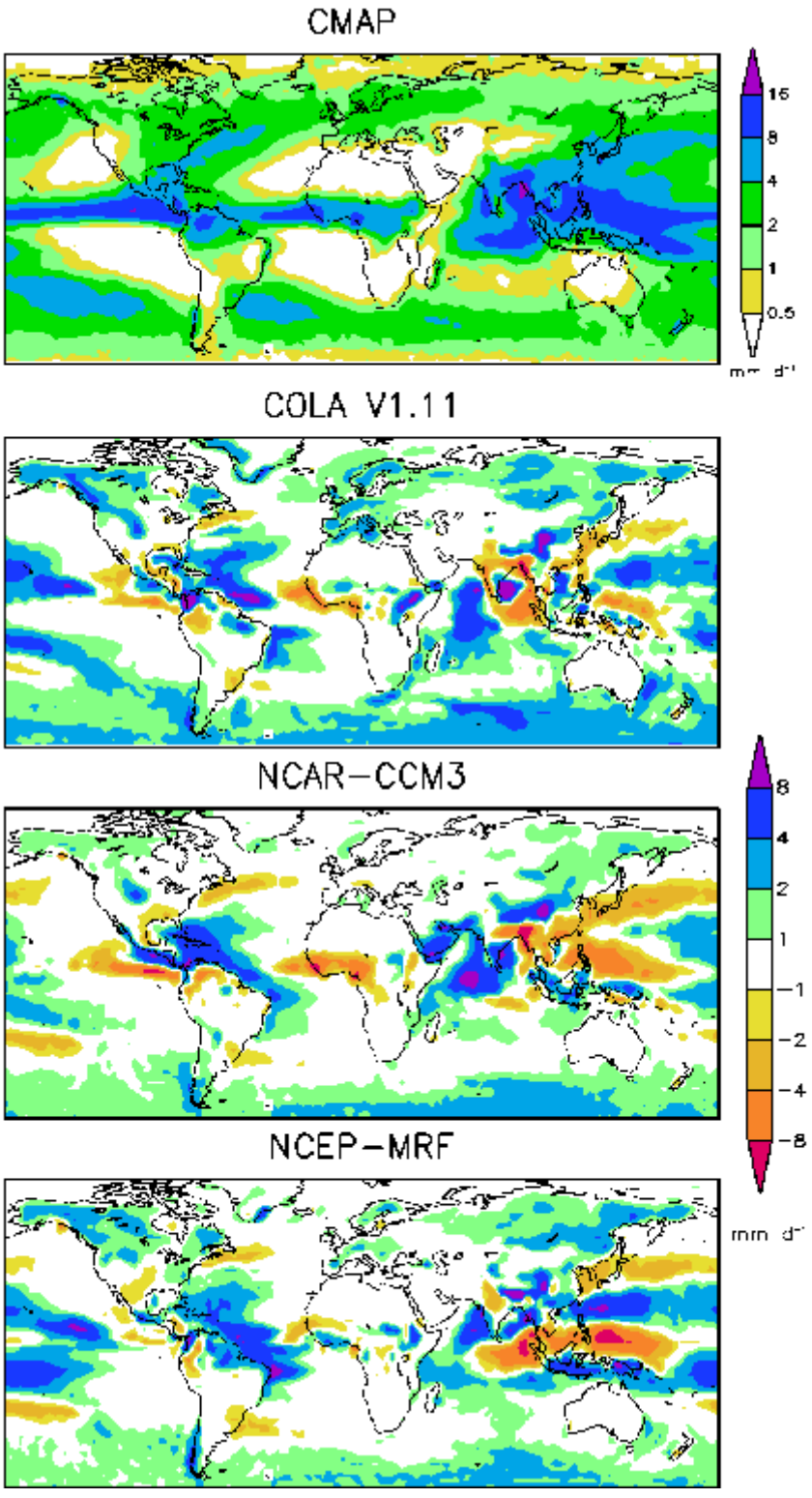

Figure 1. Observed mean JJAS precipitation averaged for the years 1986, 1987, 1988, 1993 and 1994 (top panel), and systematic errors of the three GCMs as indicated above each panel. Units are mm d^{-1}.

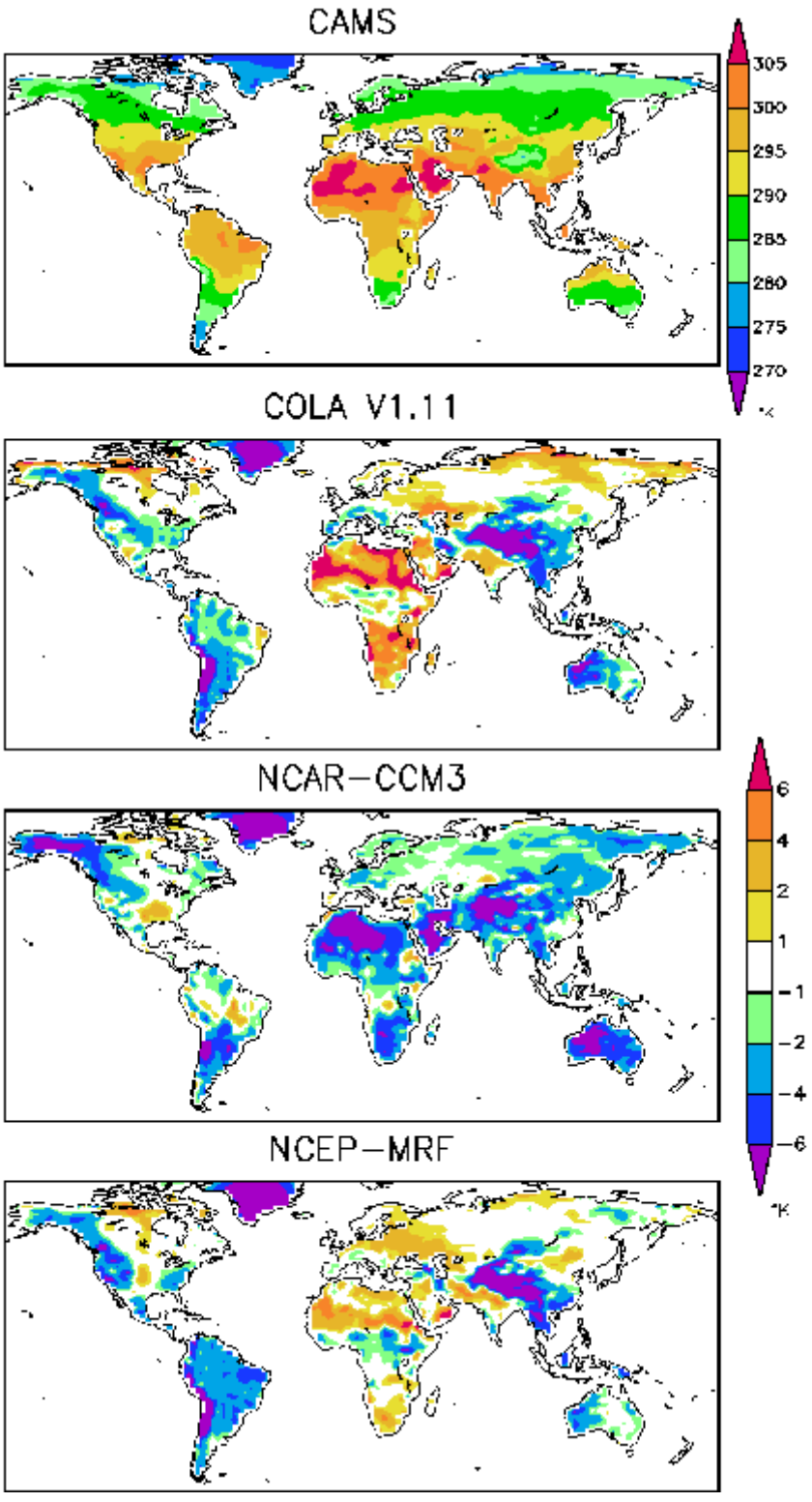

Figure 2. As in Fig. 1 for surface temperature. Units are degrees K.

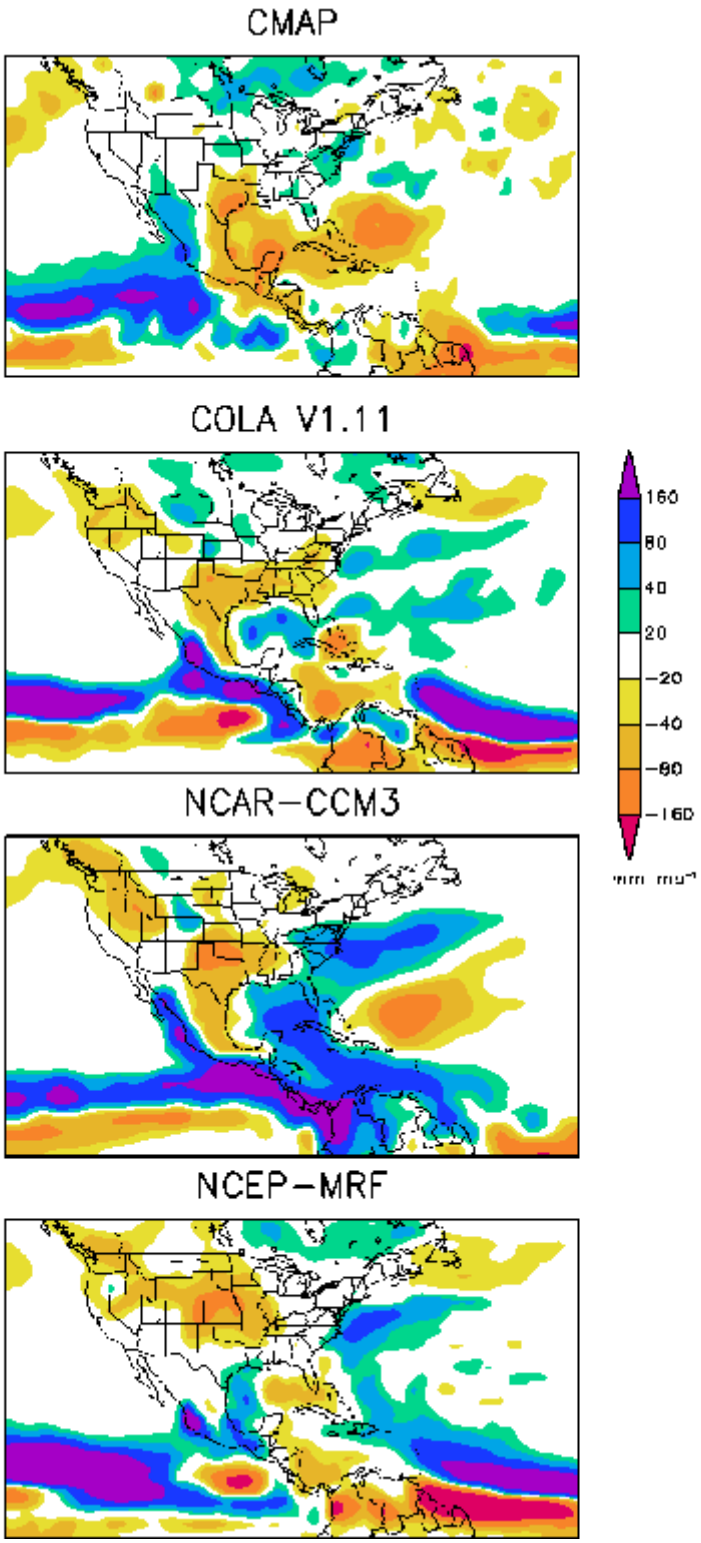

Figure 3. July minus June precipitation averaged for the years 1986, 1987, 1988, 1993 and 1994 from observations and each of the GCMs over the North American region. Units are mm d^{-1}.

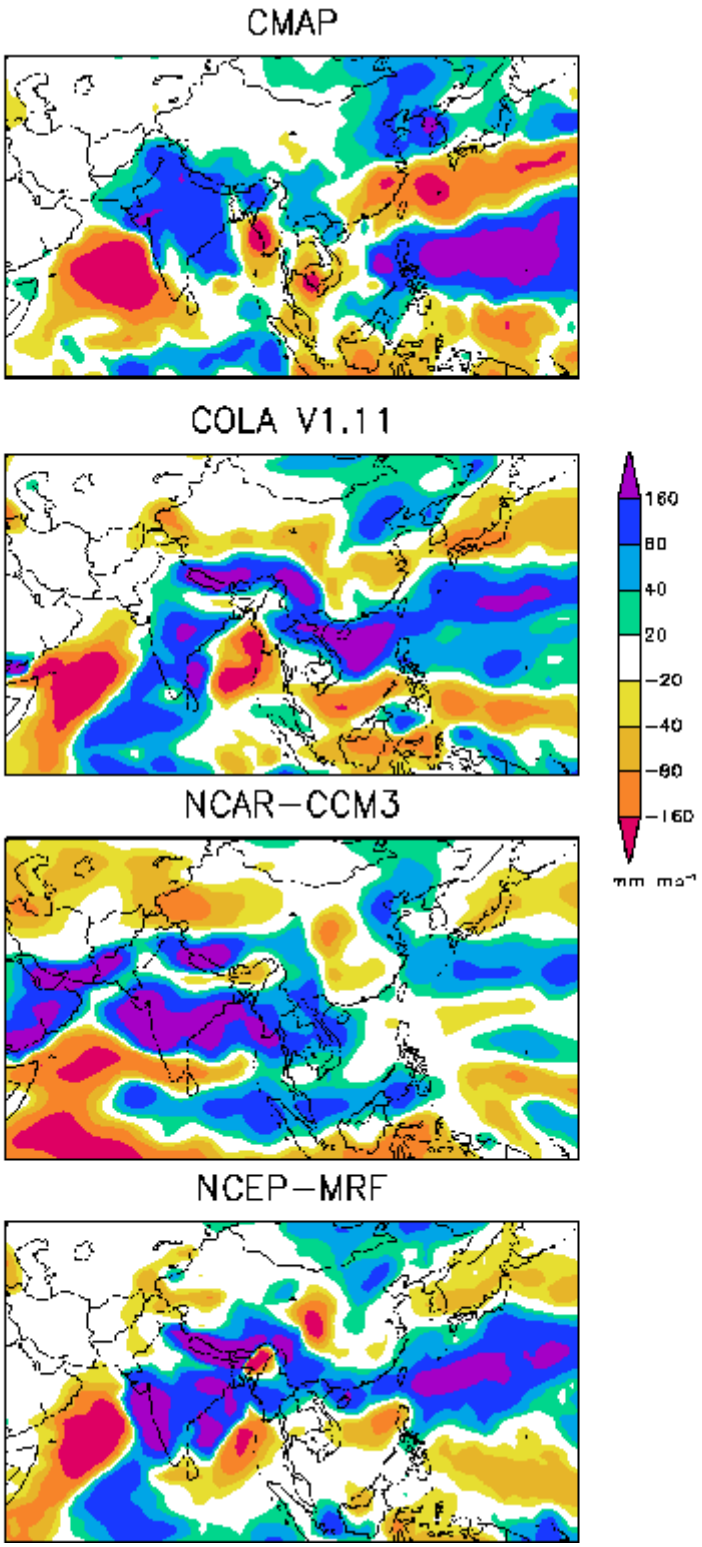

Figure 4. As in Fig 3 for southern Asia.

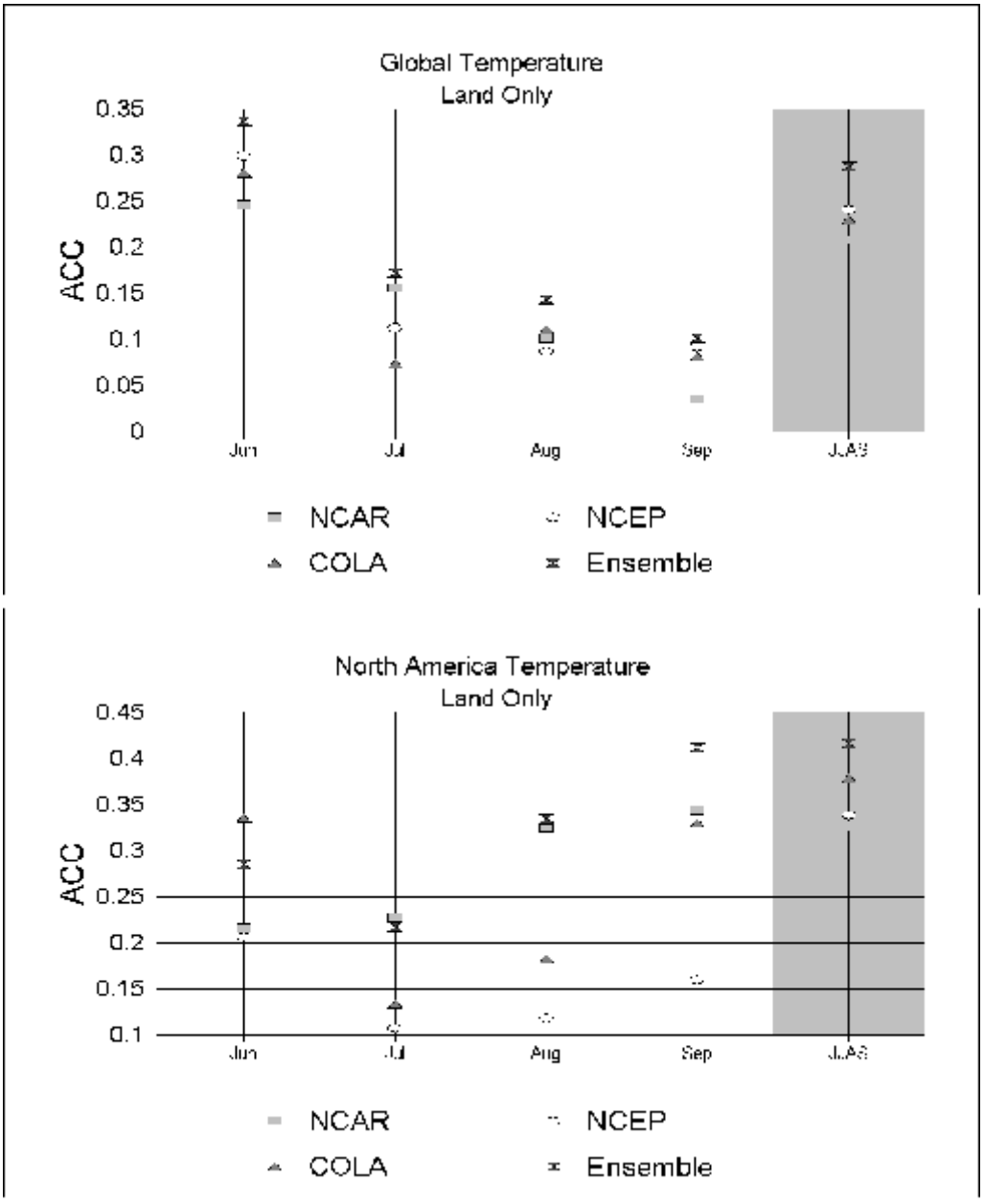

Figure 5. Mean monthly and mean seasonal spatial anomaly correlation coefficient for surface temperature for each GCM and the inter-model mean over (top) the global (60ES – 80EN) and (bottom) North American land areas. Dot-dash line indicates the 95% significance level (all points lie below this threshold for North America).

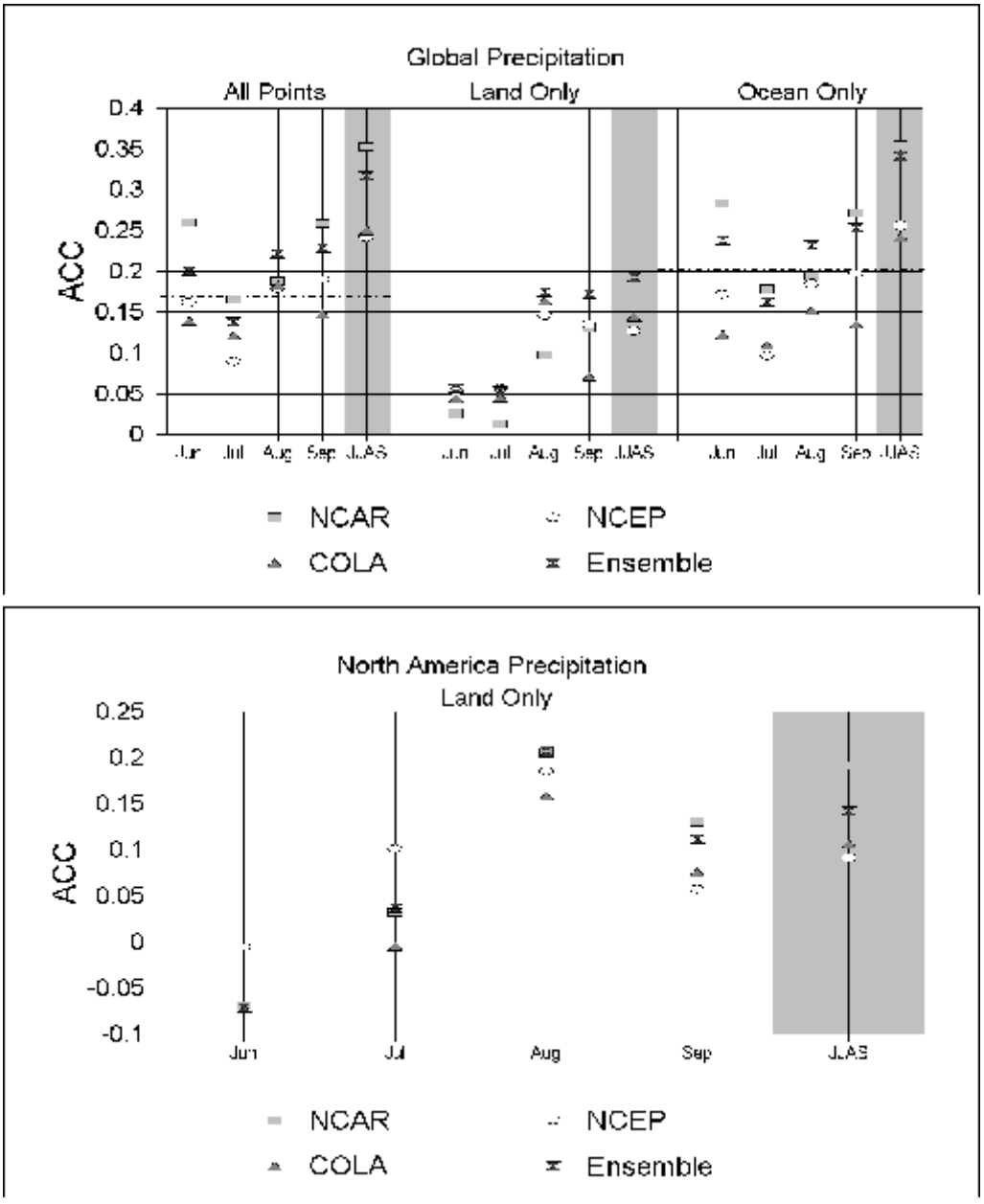

Figure 6. As in Fig 3 for precipitation. The global anomaly correlation coefficients are displayed for all points between 60ES – 80EN, land points only, and ocean points only.

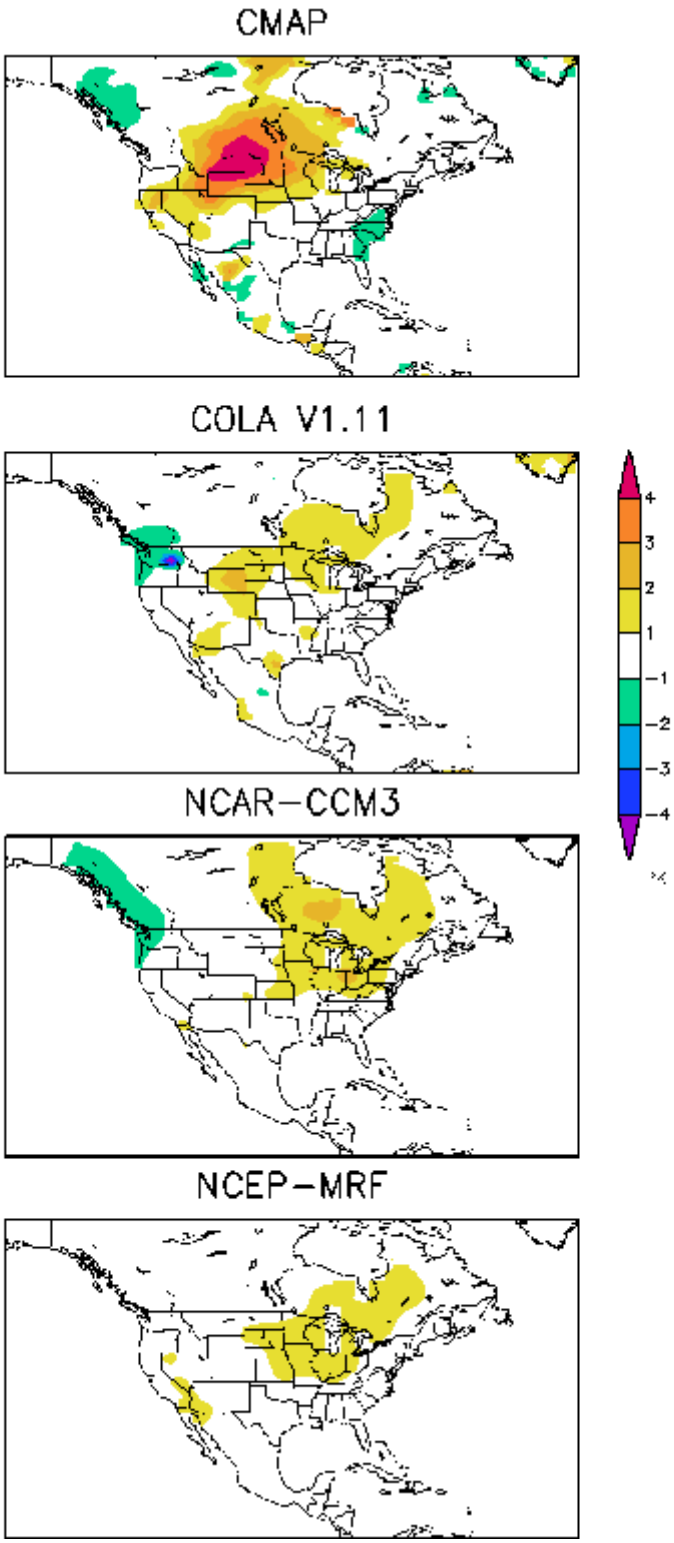

Figure 7. Mean June-July surface temperature anomaly for 1988 (compared to the other simulated years) from observations and each of the GCMs over the North American region. Units are degrees K.

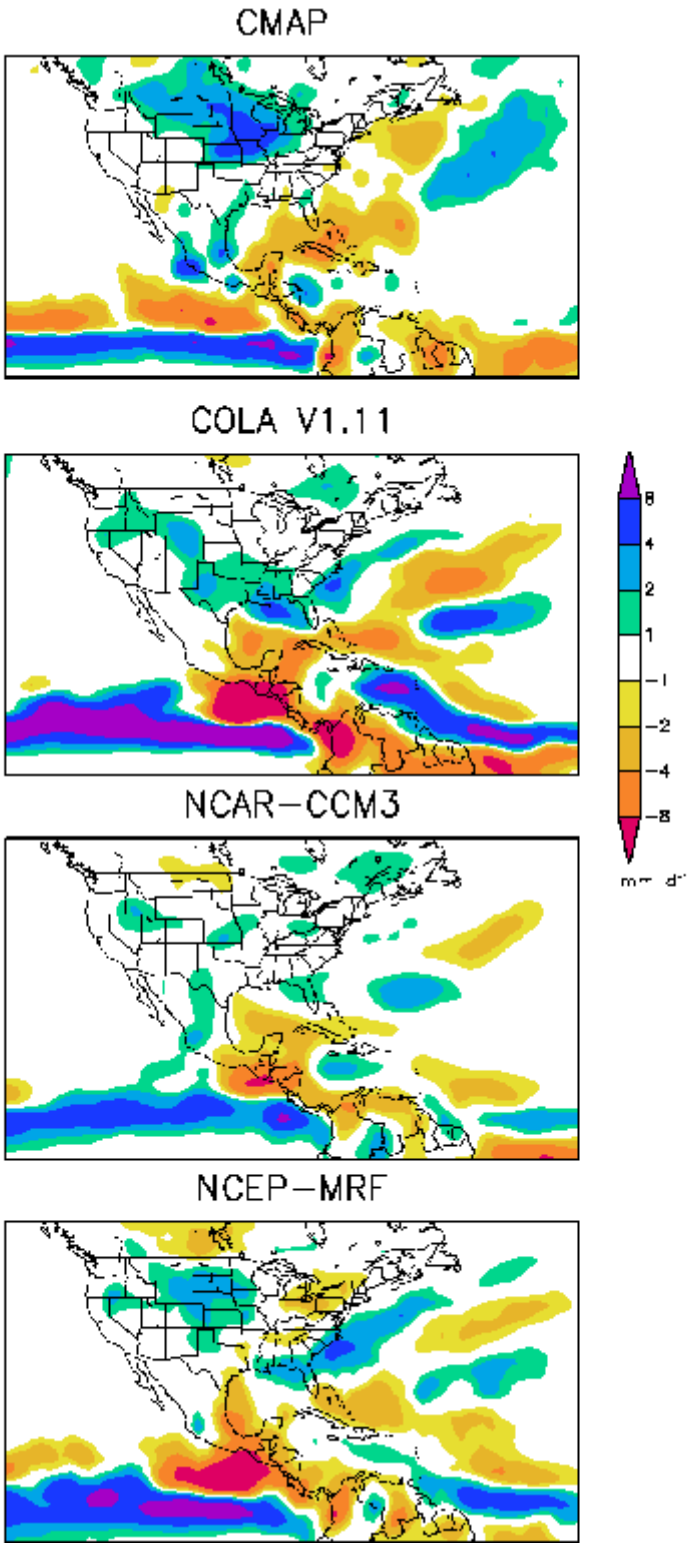

Figure 8. As in Fig 7 for 1993 minus 1998 precipitation. Units are mm d^{-1}.

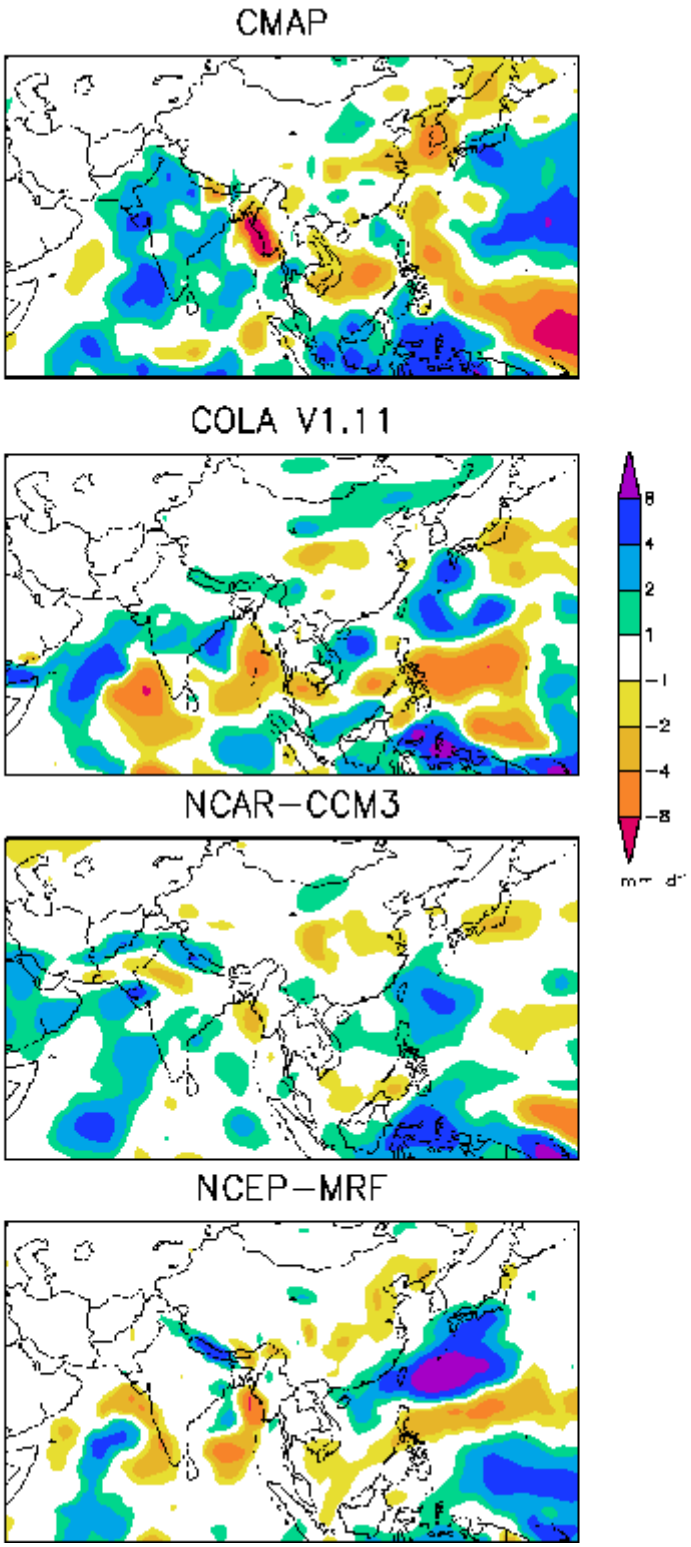

Figure 9. As in Fig 8 for 1988 minus 1987 over southern Asia.

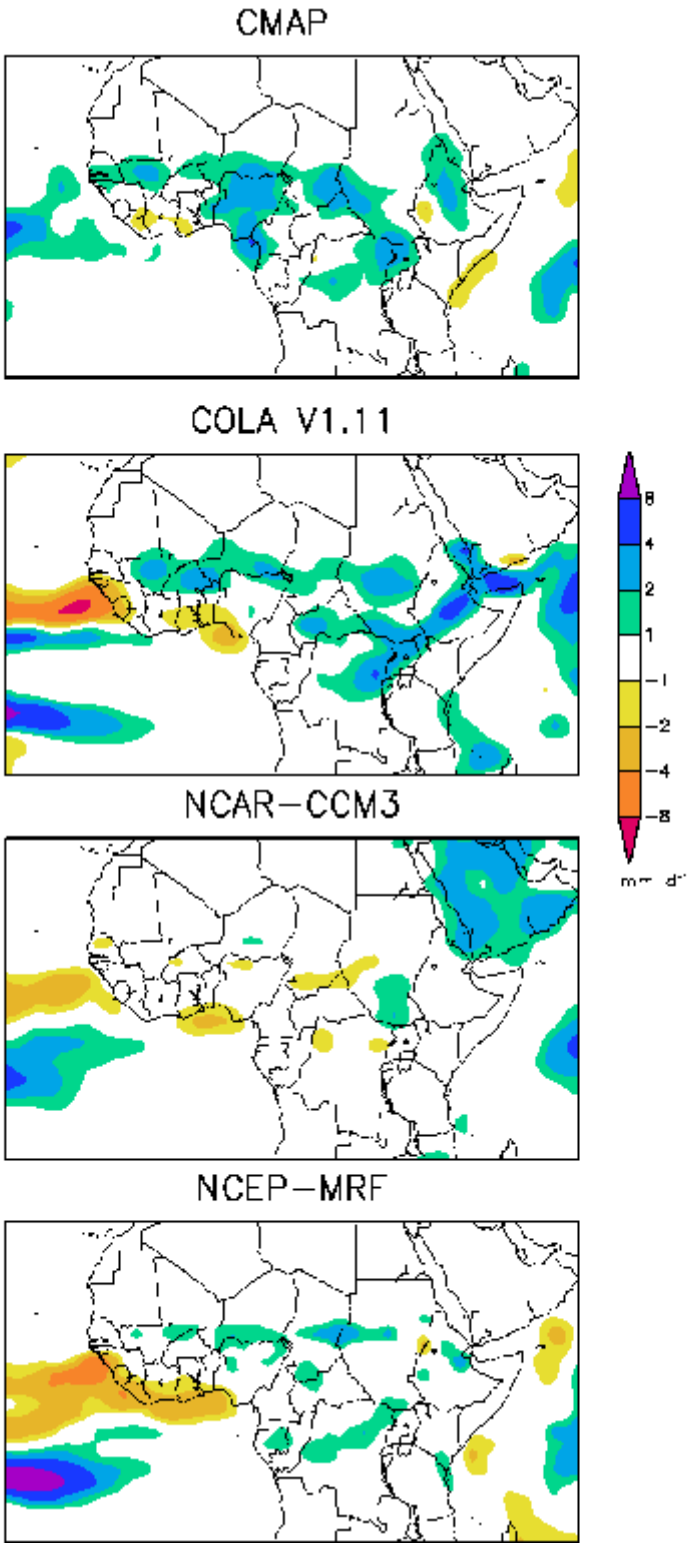

Figure 10. As in Fig 9 over Africa.

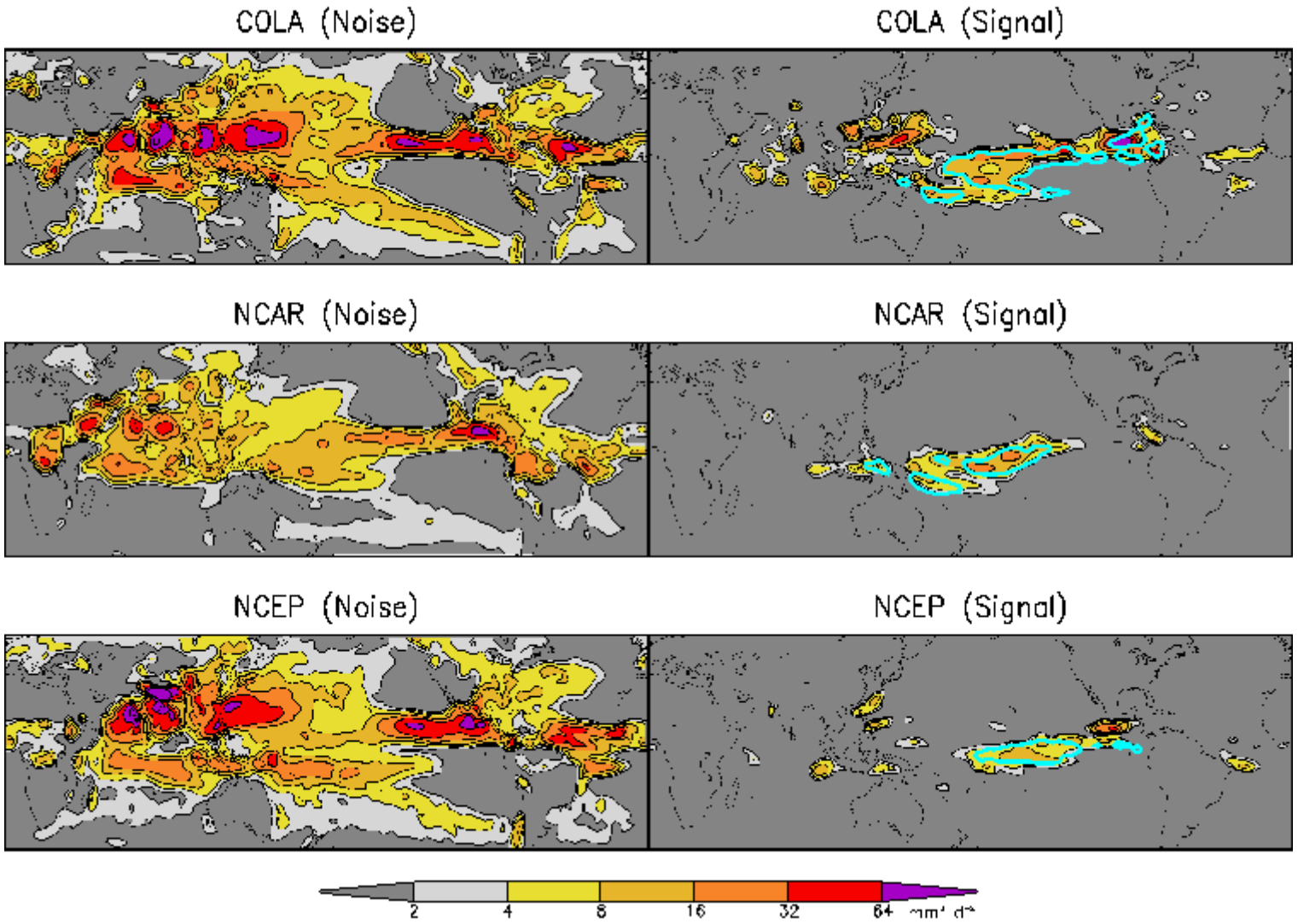

Figure 11. Noise and signal in mean JJAS precipitation as simulated by the three GCMs, following the definitions of Shukla et al. (2000). In the righthand panels, areas where signal exceeds noise are outlined by bold contours.

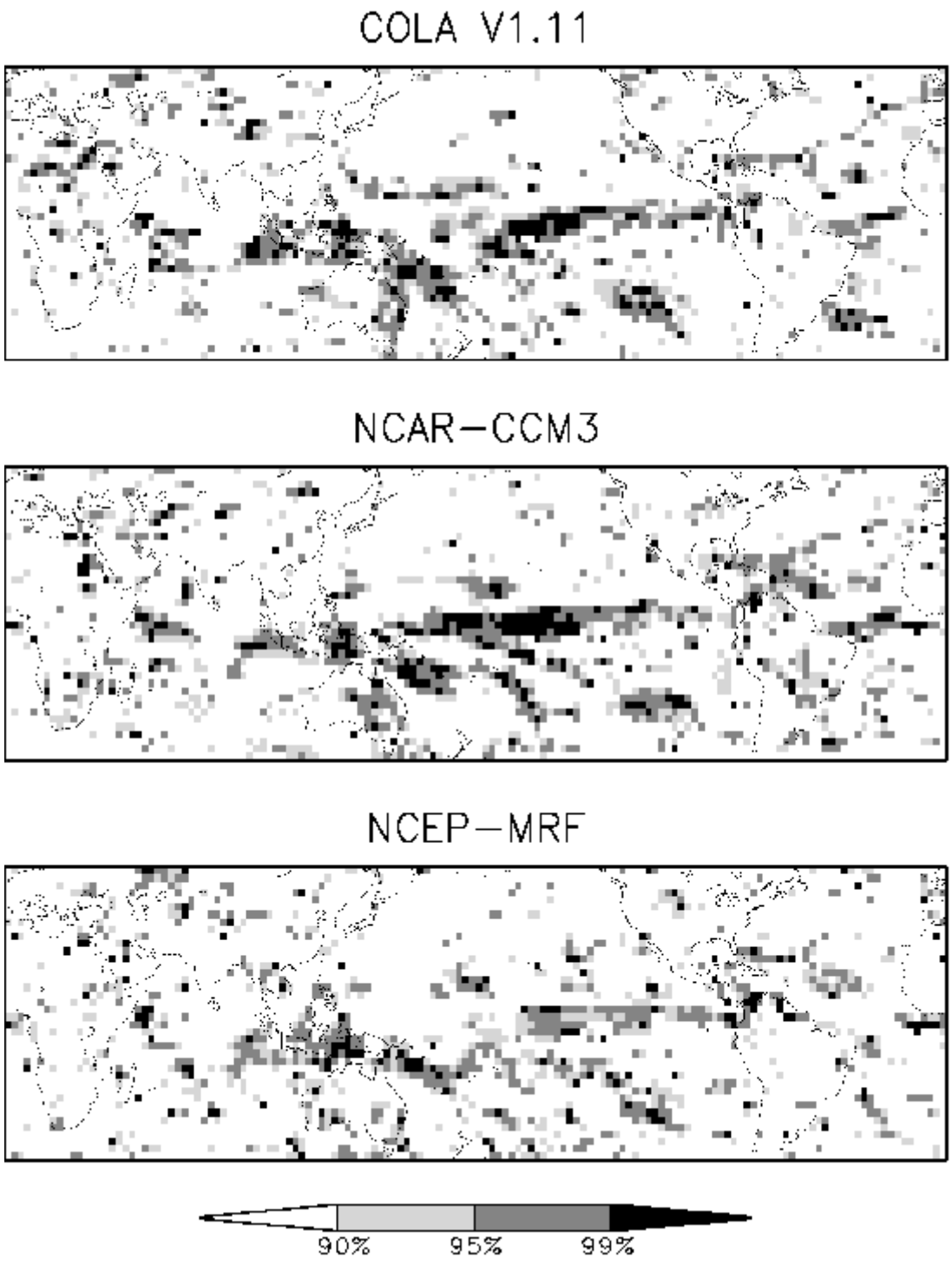

Figure 12. Interannual anomaly correlation coefficient for mean JJAS precipitation as simulated by the three GCMs.

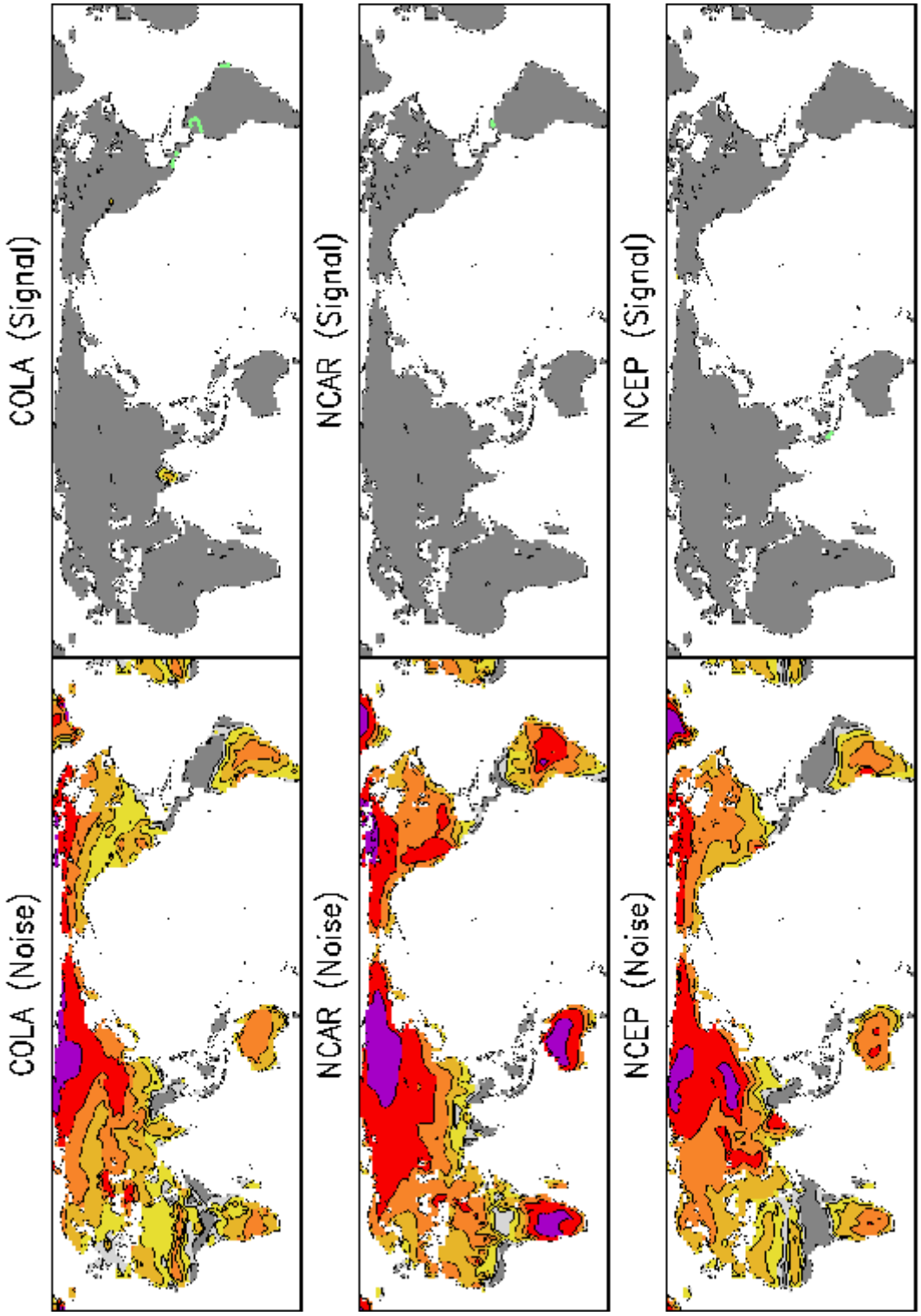

Figure 13. As in Fig. 11 for surface temperature.

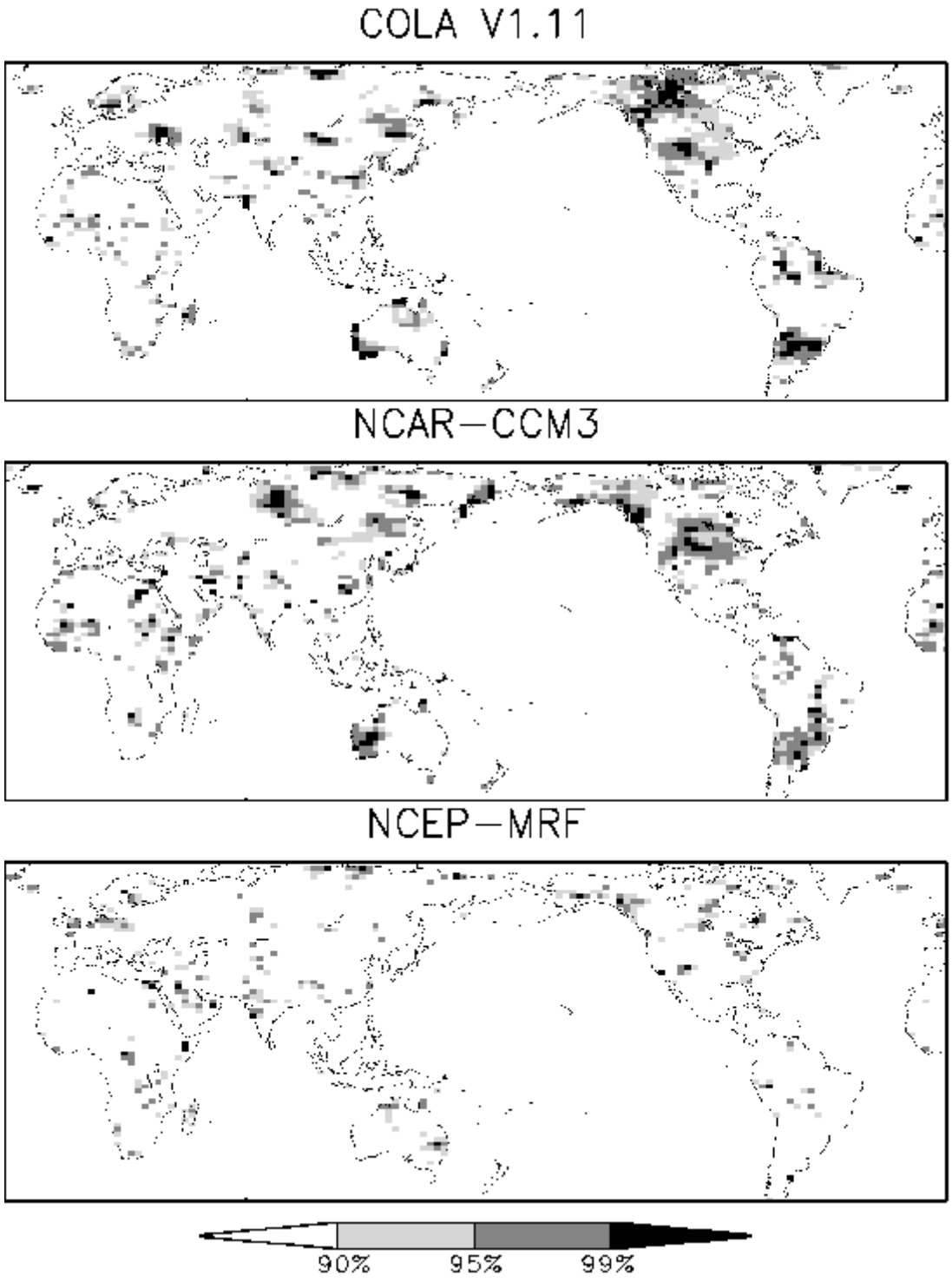

Figure 14. As in Fig. 12 for surface temperature.

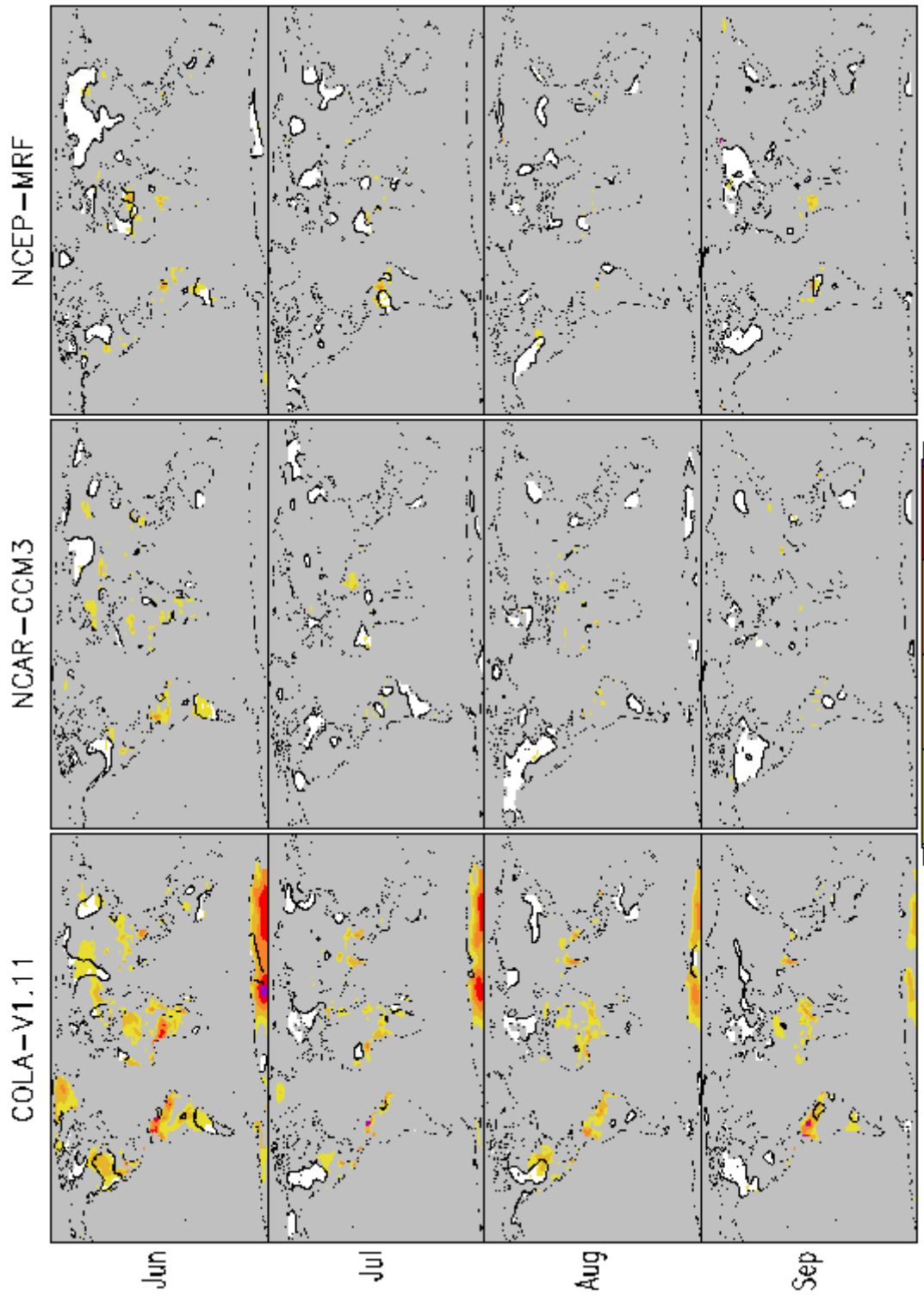

Figure 15. Signal to noise ratio (shading) and interannual anomaly correlation coefficient at the 95% confidence level (outlined) for monthly mean surface temperature for each month and GCM. Areas shaded grey have neither significant anomaly correlation nor signal exceeding noise. No calculation was performed over ocean.

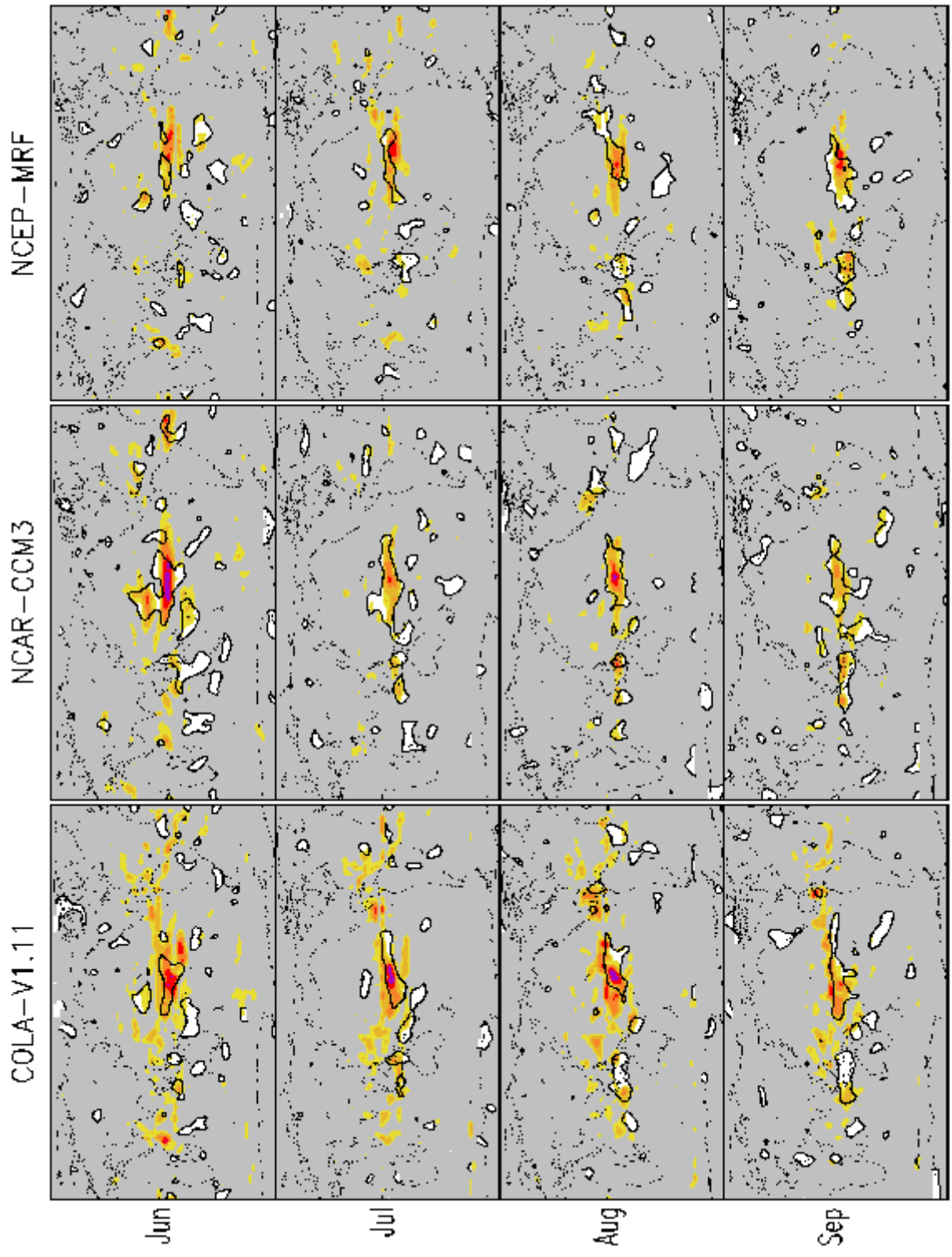

Figure 16. As if Fig. 15 for precipitation.

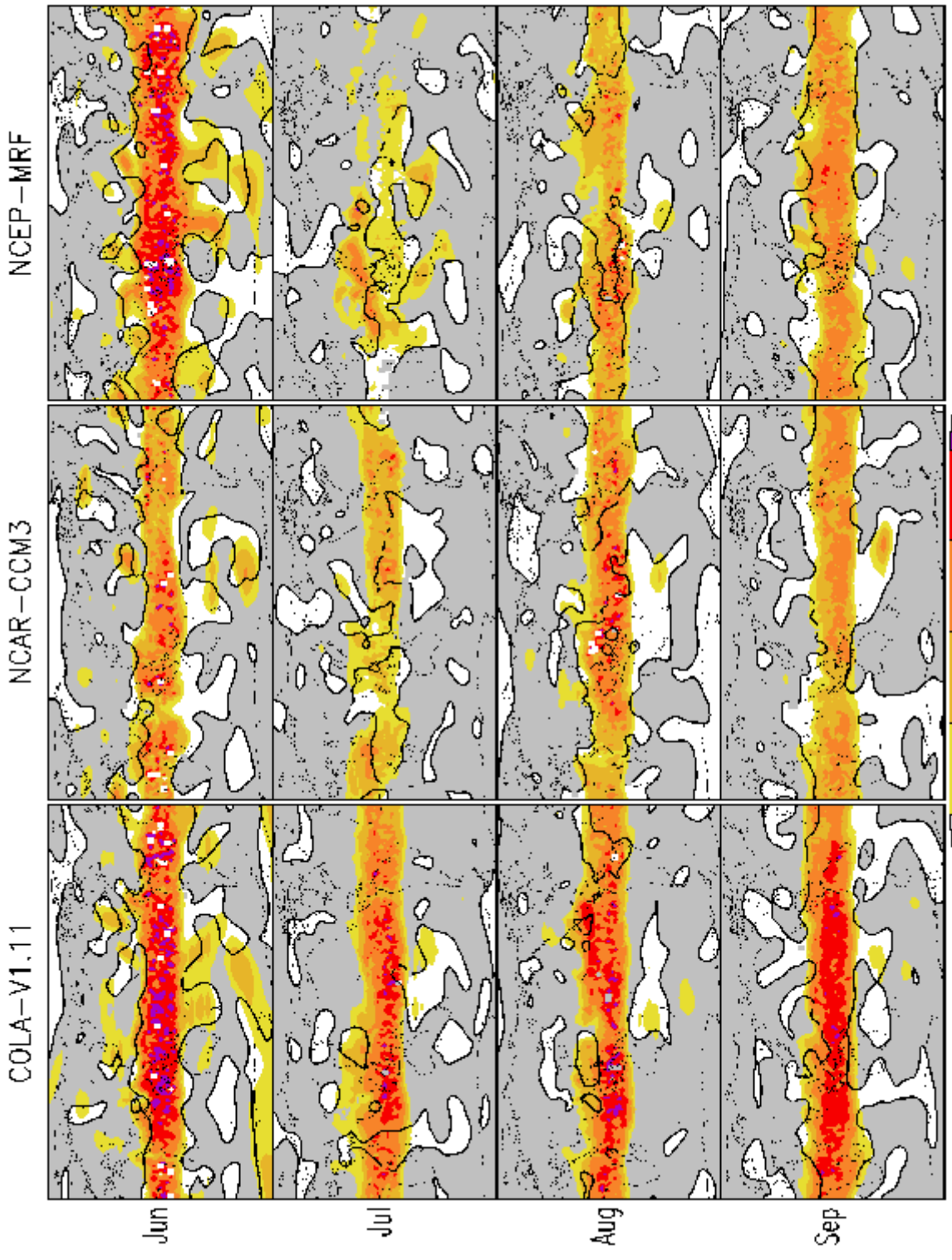

Figure 17. As in Fig. 15 for 500 hPa geopotential height.